

# Relationship between different channel light curves of gamma-ray burst pulses shown in aspects other than the pulse width

Yi-Ping Qin<sup>1,2,3</sup>

## ABSTRACT

The *FWHM* width is a well known quantity representing the characteristics of pulses of gamma-ray bursts (GRBs), for which many studies were presented. However, there are some other elements which can describe other aspects of the pulses that the width cannot. In this paper, we employ the peak count rate  $C_p$  and the total count  $C_{total}$  of light curves to study in the corresponding aspects the relationship between different channel light curves. To make a direct comparison between count rates of different channel light curves we introduce a plot of  $C(\tau)$  versus  $C_H(\tau)$ , where  $C(\tau)$  is the count rate of a channel and  $C_H(\tau)$  is the count rate of a definite channel, channel H (see the text). According to the plot we define  $\Delta C_{max}$  as the maximum deviation of the two count rate values of  $C(\tau)$  associated with a same count rate value of  $C_H(\tau)$  and define  $\Delta S$  as the area confined by the close curve of  $C(\tau)$  in the plot to measure the difference of the rising and decaying portions of a light curve relative to the count rate of channel H. Under the assumption that some GRBs observed are in the stage of fireballs which expand relativistically, predictions on the relationships between the four quantities ( $C_p$ ,  $C_{total}$ ,  $\Delta C_{max}$ , and  $\Delta S$ ) and energy within a wide band, calculated with different rest frame radiation forms and two typical Lorentz factors ( $\Gamma = 20$  and 200), are made and presented, which would make the test of our model with the coming Swift data easier. Interpretations to the relationships within the mechanism of fireballs are also presented.

*Subject headings:* gamma-rays: bursts — gamma-rays: theory — relativity

---

<sup>1</sup>National Astronomical Observatories/Yunnan Observatory, Chinese Academy of Sciences, P. O. Box 110, Kunming, Yunnan, 650011, P. R. China

<sup>2</sup>Physics Department, Guangxi University, Nanning, Guangxi 530004, P. R. China

<sup>3</sup>E-mail: ypqin@public.km.yn.cn

## 1. Introduction

Observation reveals that some simple gamma-ray bursts (GRBs) with well-separated structure consist of fundamental pulses which are seen to comprise a fast rise and an exponential decay (FRED) phases (see, e.g., Fishman et al. 1994). The FRED pulses together with the hardness-intensity correlation were interpreted as signatures of the relativistic curvature effect (the Doppler effect over the fireball surface) (Fenimore et al. 1996; Ryde and Petrosian 2002; Kocevski et al. 2003; Qin et al. 2004, hereafter Paper I). Accounting for the great output rate of radiation of GRBs, a fireball model was proposed as early as in 1980s (Goodman 1986; Paczynski 1986), and based on it, the shifting of the spectrum or the boosting of the radiation of the objects and other phenomena, due to the Doppler effect over the fireball surface, could be expected (see, e.g., Krolik and Pier 1991; Meszaros and Rees 1998; Hailey et al. 1999; Qin 2002, 2003).

One could find from the BATSE data that FRED pulse light curves of GRBs in different energy channels differ significantly in the magnitude and the width of the curves. However, from these light curves a self-similarity across energy bands could be observed (see, e.g., Norris et al. 1996). In the past few years, many attempts of interpretation of the light curves observed have been made (see, e.g., Fenimore et al. 1996; Norris et al. 1996; Norris et al. 2000; Ryde and Petrosian 2002; Kocevski et al. 2003). Statistical analysis based on the fit to the light curve revealed that the temporal scale factors of a given pulse measured at different energies are related to the corresponding energies by a power law (Fenimore et al. 1995; Norris et al. 1996; Nemiroff 2000), which was suspected to result from a relative projected speed or a relative beaming angle (Nemiroff 2000). Paper I shows that the power law relationship between the pulse width and energy as a consequence of the Doppler effect over the fireball surface is due to different active areas of the fireball surface corresponding to the majority of photons of the channels observed. An investigation on the relationship was performed in detail previously and based on it the expected behavior of the relationship in the Swift band was presented (see Qin 2004). However, the width of pulses reflects only one aspect of the light curves. Generally, for a certain event, if only a relationship is observed, one might find several mechanisms accounting for it; however, when several relationships are observed, the number of interpretation might be fewer or even unique. It is understood that, generally, the more relationships observed, the few number of possible interpretations. Therefore, to have the model completely checked or to sufficiently understand how different channel light curves are related, other quantities rather than the pulse width such as the magnitude or the total count should also be studied.

Shown in Fig. 10 of Paper I are the light curves of the four BATSE channels of GRB 951019, where the fitting curves of the four channels share the same formula with the same

parameters, differing only in the energy integral range. In this analysis, no parameters other than the energy ranges are allowed to vary with the energy channel concerned. However, even with this figure, the following question cannot easily be answered: for the same count rate of a channel measured at different times, what would happen to the count rates of other channels measured at these times? This suggests that, to show the relation between different channel light curves, figures other than this one might also be at work and might work better in some particular aspects.

In the following, we will study in detail the relation between different channel light curves with some quantities other than the width, and based on the analysis predictions on the behavior of the corresponding relationships in the Swift band will be made.

## 2. Characters of light curves determined by the energy range of channels

Through out this paper, the relation between different channel light curves of GRB pulses is studied under the assumption that the sources concerned are in the stage of fireballs which expand relativistically and isotropically. Here we study how some characters of light curves are related with the corresponding energy.

The width of pulses is a well-known character of light curves determined by energy channels. Let us consider two other quantities which are also characters of light curves associated with the corresponding channels. One is the peak count rate and the other is the total count. The distributions of these two quantities for both long and short GRBs were investigated previously (McBreen et al. 2001, 2003). Here, we pay our attention to the relations of these quantities with energy. The formula for calculating the count rate of a fireball source is (A1) (see Appendix A). In this paper, we consider only the cases of local Gaussian pulse (A2) and local power law pulse (A3) (see Appendix A). Two kinds of fireball bursts are concerned. One is a typical hard burst with  $\Gamma = 200$  and the other is a typical soft burst with  $\Gamma = 20$  and they are assumed to share the same rest frame radiation spectrum and the same local pulse (see Qin 2004). It is known that the peak energy  $E_p$  could serve as a quantity describing the hardness of the spectrum of a burst observed (see Ford et al. 1995). In the case of a rest frame Band function (Band et al. 1993) with  $\alpha_0 = -1$  and  $\beta_0 = -2.25$ , when adopting  $\nu_{0,p} = 0.75keVh^{-1}$  we find that the typical hard burst has a peak energy at  $E_p = 250keV$  and the typical soft burst is associated with  $E_p = 25keV$  (see Qin 2002 Table 4).

## 2.1. The case of a typical rest frame Band function spectrum

Here we adopt a typical Band function spectrum with  $\alpha_0 = -1$  and  $\beta_0 = -2.25$  as the rest frame radiation form to study the relation in a general manner.

The Swift telescope payload is comprised of three instruments. Two of them can detect high energy photons with one ranging from  $0.3keV$  to  $10keV$  and the other from  $15keV$  to  $150keV$  (see [http://heasarc.gsfc.nasa.gov/docs/swift/about\\_swift/](http://heasarc.gsfc.nasa.gov/docs/swift/about_swift/)). Here we study the relation within a wide band ranging from  $0.2keV$  to  $1000keV$  which covers both the Swift and BATSE bands. It should be noticed that, unlike the width of pulses, the peak and total count depend strongly on the interval of energy. We thus consider the following uniformly ranging channels (where  $E_2 = 2E_1$ ):  $[E_1, E_2] = [0.2, 0.4]keV$  (channel A),  $[0.5, 1]keV$  (channel B),  $[1, 2]keV$  (channel C),  $[2, 4]keV$  (channel D),  $[5, 10]keV$  (channel E),  $[10, 20]keV$  (channel F),  $[20, 40]keV$  (channel G),  $[50, 100]keV$  (channel H),  $[100, 200]keV$  (channel I),  $[200, 400]keV$  (channel J), and  $[500, 1000]keV$  (channel K). Note that, channel H is just the second channel of BARSE.

Shown in Fig. 1 are the light curves of all these channels for the typical hard and soft bursts, where we adopt the local Gaussian pulse with  $\Delta\tau_{\theta,FWHM} = 0.1$  and assign  $\tau_{\theta,min} = 0$  and  $\tau_{\theta,0} = 10\sigma + \tau_{\theta,min}$ . We find in the figure that while the profile of light curves is much less affected by the Lorentz factor, in agreement with what revealed in Paper I, the relative magnitudes and hence the relative total counts of different channel light curves depend strongly on the latter. Listed in Table 1 are the peak count rate  $C_p$  and the total count  $C_{total}$  of these channels associated with different local pulse forms and widths for the typical hard and soft bursts, presented in the format relative to the corresponding values of channel H. (Note that the absolute values would make sense only when all the constants concerned such as  $D$ ,  $R_c$ , and  $I_0$  are available.) It shows that relative values of these quantities depend obviously on the energy concerned as well as the adopted Lorentz factor, but they are less affected by the width and form of local pulses. Relations between the peak count rate and energy and the total count and energy associated with these channels in the case of adopting the local Gaussian pulse with  $\Delta\tau_{\theta,FWHM} = 0.1$  for the typical hard and soft bursts are displayed in Fig. 2. Shown in the figure, there exist semi-power law relationships between the peak count rate and energy and between the total count and energy for both the typical hard and soft bursts. The power law range for the hard burst covers the BATSE band while that for the soft burst spans over a much wider band, indicating that one could observe the power law relationship for the soft burst but not the hard burst in the Swift band. It seems that, for a bursts, the total count of a channel is proportional to the corresponding peak count rate. Shown in Fig. 3 are the relation between the two quantities for the typical hard and soft bursts in the case of adopting the local Gaussian pulse with  $\Delta\tau_{\theta,FWHM} = 0.1$ . A

semi-power law relationship between the two quantities is observed for both bursts, where the power law index for the hard burst is 1.34 and that for the soft one is 1.12.

One might observe that, when adopting the channels defined above, some counts such as those within  $[0.4, 0.5]keV$  would be missed. Following the way that the BATSE team adopted, one can simply consider channels not uniformly ranged but includes all the counts observed. Here, we consider another set of channels which are similar to the previous ones but include all counts. They are  $[E_1, E_2] = [0.2, 0.5]keV$  (channel Aa),  $[0.5, 1]keV$  (channel B),  $[1, 2]keV$  (channel C),  $[2, 5]keV$  (channel Da),  $[5, 10]keV$  (channel E),  $[10, 20]keV$  (channel F),  $[20, 50]keV$  (channel Ga),  $[50, 100]keV$  (channel H),  $[100, 300]keV$  (channel Ia), and  $[300, 1000]keV$  (channel Kb), where, the last four channels are just the BATSE channels. Comparing this set of channels with the previous set, one would find that channels Aa, Da, Ga, Ia, and Kb span over larger energy ranges than the corresponding channels A, D, G, I, and K do, respectively. Presented in Table 2 are the relative peak count rate and the relative total count of channels Aa, Da, Ga, Ia, and Kb arising from the local Gaussian pulse with different values of width for the typical hard and soft bursts. It shows that, due to the larger energy ranges, the two quantities of channels Aa, Da, Ga, Ia, and Kb are significantly larger than that of the corresponding channels A, D, G, I, and K, respectively. Relations between the peak count rate and energy and the total count and energy deduced from channels Aa, Da, Ga, Ia, and Kb in the case of the local Gaussian pulse with  $\Delta\tau_{\theta,FWHM} = 0.1$  for the typical hard and soft bursts are also displayed in Fig. 2. We find in the figure that the peak count rate and the total count of the channels with larger energy ranges are obviously larger than those of the smaller energy range channels, and the two quantities of the former channels form by themselves continuous relationships with energy, which are different from the relationships deduced from the smaller energy range channels. The relation between the peak count rate and total count of channels Aa, Da, Ga, Ia, and Kb arising from the local Gaussian pulse with  $\Delta\tau_{\theta,FWHM} = 0.1$  for the typical hard and soft bursts is also shown in Fig. 3. The two quantities follow almost the same power law relationships deduced from the uniformly ranging channels (channels A, B, C, D, E, F, G, H, I, J, and K).

## 2.2. The case of other rest frame radiation forms

One could observe from Tables 1 and 2 that the pulse form and width do not significantly affect the relative values of the peak count rate and total count, while the Lorentz factor does. This suggests that, when performing a statistical analysis on the relationships discussed above, the distribution of the Lorentz factor would play an important role. We wonder if the rest frame radiation form would also be an important factor in producing the relationships.

Let us study the relation in the cases of other rest frame radiation forms, where only the case of the local Gaussian pulse with  $\Delta\tau_{\theta,FWHM} = 0.1$  is considered.

Presented in Tables 3 and 4 (see Appendix B) are the relative values of the peak count rate and total count of the light curves of various channels in the case of local Gaussian pulses with  $\Delta\tau_{\theta,FWHM} = 0.1$  for two rest frame Band function spectra  $(\alpha_0, \beta_0) = (0, -3.5)$  and  $(\alpha_0, \beta_0) = (-1.5, -2)$ , respectively. We find that the impacts of the rest frame radiation form on the two quantities are very significant. Displayed in Figs. 4 and 5 are the relationships between the two quantities and energy for the two rest frame Band function spectra, respectively. We find that, for a relatively steep rest frame spectrum, there is a turnover in the relationships between the peak count rate and energy and between the total count and energy, and the relationship between the peak count rate and the total count exhibits a hook-like curve (see Fig. 4); for a relatively flat rest frame spectrum, the power law relationships between the peak count rate and energy and between the total count and energy would extend to the lower energy range of the Swift band, and the relationship between the peak count rate and the total count is a well-defined power law (see Fig. 5). From these figures one can conclude that the values of  $C_p$  and  $C_{total}$  depend obviously on the rest frame radiation form and the Lorentz factor.

Besides the Band function, two other rest frame spectra are considered. One is the thermal synchrotron spectrum which is written in the form  $I_\nu \propto (\nu/\nu_{0,s}) \exp[-(\nu/\nu_{0,s})^{1/3}]$ , where  $\nu_{0,s}$  is a constant which includes all constants in the exponential index (Liang et al. 1983). The other is the Comptonized spectrum which is written as  $I_\nu \propto \nu^{1+\alpha_{0,C}} \exp(-\nu/\nu_{0,C})$ , where  $\alpha_{0,C}$  and  $\nu_{0,C}$  are constants. Typical value  $\alpha_{0,C} = -0.6$  (Schaefer et al. 1994) for the index of the Comptonized radiation will be adopted. Corresponding to the typical hard and soft bursts, we take  $\nu_{0,s} = 3.5 \times 10^{-3} keVh^{-1}$  in the case of the rest frame thermal synchrotron spectrum (see Qin 2002 Table 3), and take  $\nu_{0,C} = 0.55 keVh^{-1}$  in the case of the rest frame Comptonized spectrum (see Qin 2002 Table 2). Relative values of the two quantities associated with various channels for these two rest frame spectra are presented in Tables 5 and 6 (see Appendix B), respectively. The values span several orders of magnitudes. Shown in Fig. 6 are the relationships between the two quantities and energy for the rest frame thermal synchrotron spectrum, which is similar to Fig. 4 where a steep form of spectra is adopted. The most obvious difference exhibits in the relationships between the peak count rate and energy and between the total count and energy associated with the typical soft burst, where the turnover is hardly detectable. The figure for the rest frame Comptonized spectrum is quite similar to Fig. 6 and therefore is omitted.

### 2.3. The case of a rest frame spectrum varying with time

Let us study the relation under the assumption that the rest frame radiation form varies with time (this phenomenon is common in observation). With the 95 bursts fitted with the Band function in Preece et al. (2000), one could find that the low and high energy power law indexes,  $\alpha$  and  $\beta$ , of the sources develop in the way  $\alpha = -0.63 - 0.20(t - t_{\min})/(t_{\max} - t_{\min})$  and  $\beta = -2.44 - 0.42(t - t_{\min})/(t_{\max} - t_{\min})$  in terms of statistics (see Qin 2004). We therefore consider an evolution of the rest frame indexes  $\alpha_0$  and  $\beta_0$  following  $\alpha_0 = -0.63 - 0.20(\tau_\theta - \tau_{\theta,\min})/(\tau_{\theta,\max} - \tau_{\theta,\min})$  and  $\beta_0 = -2.44 - 0.42(\tau_\theta - \tau_{\theta,\min})/(\tau_{\theta,\max} - \tau_{\theta,\min})$ . Here, the relation will be studied in the case of adopting the local Gaussian pulse with  $\Delta\tau_{\theta,FWHM} = 0.1$ . We thus use  $6\sigma$  to replace  $\tau_{\theta,\max} - \tau_{\theta,\min}$  in these two relations. In the same way, we take  $\nu_{0,p} = 0.75\text{keV}h^{-1}$  and assign  $\Gamma = 200$  to the hard burst and  $\Gamma = 20$  to the soft one. Associated with the decreasing of the indexes, we ignore the rising portion of the local pulse and assign for the local Gaussian pulse that  $\tau_{\theta,0} = \tau_{\theta,\min}$  and  $\tau_{\theta,\min} = 0$ . Listed in Table 7 (see Appendix B) are the relative values of the peak count rate and total count of the light curves of various channels in the case of local Gaussian pulses with  $\Delta\tau_{\theta,FWHM} = 0.1$  for the rest frame varying Band function spectrum. The values also span several orders of magnitudes. The figure showing the relationships between the two quantities and energy for the rest frame varying Band function spectrum is also similar to Fig. 4 (it is therefore omitted), suggesting that, creating the relation between different channel light curves, the rest frame varying Band function acts like a steep form of rest frame spectra.

## 3. Direct comparison between count rates of different channel light curves

In this section we make a direct comparison between count rates of different channel light curves, which may reveal other aspects of the relation between them. All channels discussed above will be concerned.

### 3.1. The case of a typical rest frame Band function spectrum

Here we consider a rest frame Band function spectrum with  $\alpha_0 = -1$  and  $\beta_0 = -2.25$ .

Presented in Fig. 7 are the curves of  $C(\tau)$  versus  $C_H(\tau)$  deduced from the light curves of Fig.1, where  $C_H(\tau)$  is the count rate of channel H. This figure would be able to tell if the rising or decaying speeds of the light curves of different channels are the same. We find that, generally, the speeds are not the same, and for each channel, the rising and decaying parts of  $C(\tau)$  in the figure constitute a close curve. For the typical soft burst, the speed of rising

or decaying of the count rate of higher energy bands is the same for different channels while the speed in lower energy bands varies significantly. Corresponding to a certain value of the count rate of channel H, there are two values of the count rate of lower energy channels, where the one associated with the rising portion of the light curve is larger than the one associated with the decaying phase. This bi-valued character can also be seen in the case of the typical hard burst, where for higher energy channels the one associated with the rising portion of the light curve is smaller than the one associated with the decaying phase. Besides the peak count rate discussed above, there are two characters of the close curves in Fig. 7. One is the maximum value of the deviation of the two values of the count rate of a channel corresponding to a certain value of that of channel H. The other is the area confined by each close curve in the figure. We define the maximum deviation of the two count rates of a channel corresponding to a certain count rate of channel H as  $\Delta C_{\max} \equiv C_r/C_{p,H} - C_d/C_{p,H}$  when  $|C_r/C_{p,H} - C_d/C_{p,H}|$  is maximum, where  $C_r$  and  $C_d$  are the count rates of the rising portion and decaying phase of the light curve, respectively, and  $C_{p,H}$  is the peak count rate of channel H. In addition, we define an area  $\Delta S$  confined by the close curve as the area under the rising portion curve minus that under the decaying phase curve in the plot of  $C(\tau)$  versus  $C_H(\tau)$ , where all count rates are normalized to  $C_{p,H}$  (see Fig. 7). According to their definition, the values of both  $\Delta C_{\max}$  and  $\Delta S$  can be positive or negative. Presented in Table 8 are the values of  $\Delta C_{\max}$  and  $\Delta S$  associated with different channel light curves in the case of local Gaussian pulses with various values of  $\Delta\tau_{\theta,FWHM}$  for the rest frame Band function spectrum with  $\alpha_0 = -1$  and  $\beta_0 = -2.25$ . We find that to determine these two quantities the Lorentz factor plays an important role while the width of local pulses does not. Displayed in Fig. 8 are the relationships between  $\Delta C_{\max}$  and energy, and between  $\Delta S$  and energy, and between  $\Delta C_{\max}$  and  $\Delta S$  themselves. It shows that, generally, both  $\Delta C_{\max}$  and  $\Delta S$  increase with the increasing of energy, and in the relationships between  $\Delta C_{\max}$  and  $\log E/keV$  and between  $\Delta S$  and  $\log E/keV$ , a turnover will be observed in the case of the typical hard burst and a platform will be seen in the case of the typical soft burst in a higher energy range. The two quantities are linearly correlated. The slope for the typical hard burst is 0.70 while that for the typical soft burst is 0.72.

### 3.2. The case of other rest frame spectra

The cases of other rest frame spectra discussed above are studied here, including: two rest frame Band function spectra with  $(\alpha_0, \beta_0) = (0, -3.5)$  and  $(\alpha_0, \beta_0) = (-1.5, -2)$ , respectively; the thermal synchrotron spectrum  $I_\nu \propto (\nu/\nu_{0,s}) \exp[-(\nu/\nu_{0,s})^{1/3}]$ ; the Comptonized spectrum  $I_\nu \propto \nu^{1+\alpha_{0,C}} \exp(-\nu/\nu_{0,C})$ ; and a varying Band function with its indexes changing following  $\alpha_0 = -0.63 - 0.20(\tau_\theta - \tau_{\theta,\min})/(\tau_{\theta,\max} - \tau_{\theta,\min})$  and  $\beta_0 = -2.44 - 0.42(\tau_\theta -$



$\tau_{\theta,\min})/(\tau_{\theta,\max} - \tau_{\theta,\min})$ . We will take the same parameters adopted above to calculate the two quantities  $\Delta C_{\max}$  and  $\Delta S$ . Listed in Tables 9-13 (see Appendix B) are the values of  $\Delta C_{\max}$  and  $\Delta S$  calculated in the case of the local Gaussian pulse with  $\Delta\tau_{\theta,FWHM} = 0.1$ , adopting these rest frame spectra. It shows that, to produce  $\Delta C_{\max}$  and  $\Delta S$ , the Lorentz factor plays an important role. It is interesting that, for the typical soft burst the values of  $\Delta C_{\max}$  and  $\Delta S$  span over one order of magnitudes, while for the typical hard burst they vary mildly. This suggests that, for a certain radiation form, the ranges of  $\Delta C_{\max}$  and  $\Delta S$  are sensitive to the Lorentz factor. Shown in Figs. 9-13 are the relationship between  $\Delta C_{\max}$  and energy associated with these rest frame spectra (the relationship between  $\Delta S$  and energy is not presented in these figures due to the similarity to the relationship between  $\Delta C_{\max}$  and energy). The linear relationship between  $\Delta C_{\max}$  and  $\Delta S$  is almost the same for different cases discussed here and therefore the corresponding figures are omitted. For a relatively flat rest frame spectrum,  $\Delta C_{\max}$  increases with energy, where a platform in the high energy range can be observed (see Fig. 10). The platform shifts to lower energy bands when the Lorentz factor becomes smaller. For a relatively steep rest frame spectrum,  $\Delta C_{\max}$  decreases with energy in lower bands while increases in higher bands. For the typical soft burst, there is a platform in the higher bands, while for the typical hard burst, the platform is replaced by a convex curve (see Fig. 9). Exhibited in the relationship, the behavior of the rest frame thermal synchrotron, Comptonized and the varying Band function spectra is similar to that of the rest frame steep spectrum (see Figs. 9 and 11-13). The values of the two quantities rely obviously on the rest frame radiation form.

#### 4. Discussion and conclusions

In this paper, the relation between different channel light curves of GRB pulses is studied in aspects other than the width of pulses. The peak count rate  $C_p$  and the total count  $C_{total}$  are employed. To make a direct comparison between count rates of different channel light curves we introduce a plot of  $C(\tau)$  versus  $C_H(\tau)$ , where  $C(\tau)$  is the count rate of a channel and  $C_H(\tau)$  is the count rate of channel H. According to the plot we define  $\Delta C_{\max}$  as the maximum deviation of the two count rate values of  $C(\tau)$  associated with a same count rate value of  $C_H(\tau)$  and define  $\Delta S$  as the area confined by the close curve of  $C(\tau)$  in the plot to measure the difference of the rising and decaying portions of a light curve relative to the count rate of channel H. Predictions on the four quantities  $C_p$ ,  $C_{total}$ ,  $\Delta C_{\max}$ , and  $\Delta S$  within the Swift band, calculated with different rest frame radiation forms and two typical Lorentz factors, are made and presented (see the tables), which would make the test of our model with the coming Swift data easier.

As shown in Fig. 7, a positive value of  $\Delta C_{\max}$  (or  $\Delta S$ ) suggests that the ratio of  $C(\tau)$  to  $C_H(\tau)$  in the rising portion of  $C(\tau)$  is generally larger than that in the decaying phase, and a negative value of  $\Delta C_{\max}$  (or  $\Delta S$ ) means the opposite.

The analysis shows that the four quantities  $C_p$ ,  $C_{total}$ ,  $\Delta C_{\max}$ , and  $\Delta S$  depend obviously on energy. The relationships between them and energy are not significantly affected by the local pulse form and width. Instead, they rely on the Lorentz factor and the rest frame radiation form.

In the case of a relatively flat rest frame spectrum, both  $C_p$  and  $C_{total}$  decrease with energy (see Fig. 5). As the radiation form is not significantly affected by the Doppler effect of fireballs (see Qin 2002), we suspect that this trend might be a consequence of the relatively large amount of rest frame low energy photons which shift to X-ray or low gamma-ray bands. In the case of a relatively steep rest frame spectrum, there is a turnover in the relationship between  $C_p$  (or  $C_{total}$ ) and energy (see Figs. 4 and 6). This might be caused by the position of the peak energy  $E_p$  of the observed spectrum. As the spectrum is steep, the number of both higher and lower energy photons must be relatively small, and the peak count rate would be observed in the channel around  $E_p$ . Indeed, we find in Figs. 4 and 6 that the turnover appears in higher energy band when the Lorentz factor is large (note that  $E_p \propto \Gamma$ ; see, e.g., Qin 2002).

Shown in Figs. 9-13 we find that the value of  $\Delta C_{\max}$  is negative in low energy bands. This suggests that, compared with those of channel H, both the increasing speed of the low energy photon number in the rising phase and the decreasing speed of the number in the decaying phase are smaller. We regard this as a consequence of the expanding fireball, where high energy photons mainly come from the small area close to the line of sight and hence the number of the photons increases rapidly while low energy photons come from both the small area close to the line of sight and most of the rest area of the fireball surface and hence the number of the photons increases slowly, and for the same reason the number of high energy photons decreases rapidly while the number of low energy photons decreases slowly in the decaying phase.

This work was supported by the Special Funds for Major State Basic Research Projects (“973”) and National Natural Science Foundation of China (No. 10273019).

### A. Formulas used throughout this paper

Formulas used throughout this paper can be found elsewhere (e.g., Qin 2004). They are presented in the following so that it would be convenient to employ them (e.g., when parameters of the formulas are concerned).

In this paper, we consider a highly symmetric and relativistically expanding fireball emitting when (internal or external) shocks occur. As shown in Qin (2004), the expected count rate of a fireball expanding with a Lorentz factor  $\Gamma > 1$ , measured within frequency interval  $[\nu_1, \nu_2]$ , can be determined by

$$C(\tau) = \frac{2\pi R_c^2}{hD^2} \frac{\int_{\tilde{\tau}_{\theta,\min}}^{\tilde{\tau}_{\theta,\max}} [\tilde{I}(\tau_\theta)(1 + \beta\tau_\theta)^2(1 - \tau + \tau_\theta) \int_{\nu_1}^{\nu_2} \frac{g_{0,\nu}(\nu_{0,\theta})}{\nu} d\nu] d\tau_\theta}{\Gamma^3(1 - \beta)^2(1 + \frac{\beta}{1-\beta}\tau)^2}, \quad (\text{A1})$$

with  $\tau_{\min} \leq \tau \leq \tau_{\max}$ ,  $\tau_{\min} \equiv (1 - \beta)\tau_{\theta,\min}$ ,  $\tau_{\max} \equiv 1 + \tau_{\theta,\max}$ ,  $\tau \equiv (t - \frac{D}{c} + \frac{R_c}{c} - t_c)/\frac{R_c}{c}$ , and  $\tau_\theta \equiv (t_\theta - t_c)/\frac{R_c}{c}$ , where  $t$  is the observation time measured by the distant observer,  $t_\theta$  is the local time measured by the local observer located at the place encountering the expanding fireball surface at the position of  $\theta$  relative to the center of the fireball,  $t_c$  is the initial local time,  $R_c$  is the radius of the fireball measured at  $t_\theta = t_c$ ,  $D$  is the distance from the fireball to the observer,  $\tilde{I}(\tau_\theta)$  represents the development of the intensity measured by the local observer, and  $g_{0,\nu}(\nu_{0,\theta})$  describes the rest frame radiation, and  $\nu_{0,\theta} = (1 - \beta + \beta\tau)\Gamma\nu/(1 + \beta\tau_\theta)$ ,  $\tilde{\tau}_{\theta,\min} = \max\{\tau - 1, \tau_{\theta,\min}\}$ , and  $\tilde{\tau}_{\theta,\max} = \min\{\tau/(1 - \beta), \tau_{\theta,\max}\}$ , with  $\tau_{\theta,\min}$  and  $\tau_{\theta,\max}$  being the upper and lower limits of  $\tau_\theta$ , respectively, which confine  $\tilde{I}(\tau_\theta)$ . (Note that, since the limit of the Lorentz factor is  $\Gamma > 1$ , the formula can be applied in the cases of relativistic, sub-relativistic, and non-relativistic motions.)

We consider in this paper two kinds of local pulses. The first is a local Gaussian pulse. The intensity is assumed to be

$$\tilde{I}(\tau_\theta) = I_0 \exp[-(\frac{\tau_\theta - \tau_{\theta,0}}{\sigma})^2] \quad (\tau_{\theta,\min} \leq \tau_\theta), \quad (\text{A2})$$

where  $I_0$ ,  $\sigma$ ,  $\tau_{\theta,0}$  and  $\tau_{\theta,\min}$  are constants. As shown in Paper I, there is a constraint to the lower limit of  $\tau_\theta$ . Due to this constraint, it is impossible to take a negative infinity value of  $\tau_{\theta,\min}$  and therefore the interval between  $\tau_{\theta,0}$  and  $\tau_{\theta,\min}$  must be limited. We hence assign  $\tau_{\theta,0} = 10\sigma + \tau_{\theta,\min}$  so that the interval between  $\tau_{\theta,0}$  and  $\tau_{\theta,\min}$  would be large enough to make the rising part of the local pulse close to that of the Gaussian pulse. The *FWHM* width of the Gaussian pulse is  $\Delta\tau_{\theta,FWHM} = 2\sqrt{\ln 2}\sigma$ , which leads to  $\sigma = \Delta\tau_{\theta,FWHM}/2\sqrt{\ln 2}$ . The second is a local pulse with a power law rise and a power law decay, which is assumed to be

$$\tilde{I}(\tau_\theta) = I_0 \left\{ \begin{array}{ll} (\frac{\tau_\theta - \tau_{\theta,\min}}{\tau_{\theta,0} - \tau_{\theta,\min}})^\mu & (\tau_{\theta,\min} \leq \tau_\theta \leq \tau_{\theta,0}) \\ (1 - \frac{\tau_\theta - \tau_{\theta,0}}{\tau_{\theta,\max} - \tau_{\theta,0}})^\mu & (\tau_{\theta,0} < \tau_\theta \leq \tau_{\theta,\max}) \end{array} \right\}, \quad (\text{A3})$$

where  $I_0$ ,  $\mu$ ,  $\tau_{\theta,\min}$ ,  $\tau_{\theta,0}$  and  $\tau_{\theta,\max}$  are constants. The peak of this intensity is at  $\tau_{\theta,0}$ , and the two *FWHM* positions of this intensity before and after  $\tau_{\theta,0}$  are  $\tau_{\theta,FWHM1} = 2^{-1/\mu}\tau_{\theta,0} + (1 - 2^{-1/\mu})\tau_{\theta,\min}$  and  $\tau_{\theta,FWHM2} = 2^{-1/\mu}\tau_{\theta,0} + (1 - 2^{-1/\mu})\tau_{\theta,\max}$ , respectively. In the case of  $\mu = 2$ , the *FWHM* width of this local pulse is  $\Delta\tau_{\theta,FWHM} = (1 - 1/\sqrt{2})(\tau_{\theta,\max} - \tau_{\theta,\min})$ , which leads to  $\tau_{\theta,\max} = \Delta\tau_{\theta,FWHM}/(1 - 1/\sqrt{2}) + \tau_{\theta,\min}$ .

Through out this paper, we take  $\tau_{\theta,\min} = 0$ , and in the case of the local power law pulse we take  $\mu = 2$  and assign  $\tau_{\theta,0} = \tau_{\theta,\max}/2$  (in the case of the rest frame varying Band function spectrum, we assign  $\tau_{\theta,0} = \tau_{\theta,\min}$ ).

## B. Some tables

Tables 3-7 and 9-13 are presented here in case of being useful when one is able to check the predictions with these tables and observational data.

## REFERENCES

- Band, D., Matteson, J., Ford, L. et al. 1993, ApJ, 413, 281
- Fenimore, E. E., in’t Zand, J. J. M., Norris, J. P. et al. 1995, ApJ, 448, L101
- Fenimore, E. E., Madras, C. D., Nayakshin, S. 1996, ApJ, 473, 998
- Fishman, G. J., Meegan, C. A., Wilson, R. B. et al. 1994, ApJS, 92, 229
- Ford, L. A., Band, D. L., Matteson, J. L., et al. 1995, ApJ, 439, 307
- Goodman, J. 1986, ApJ, 308, L47
- Hailey, C. J., Harrison, F. A., Mori, K. 1999, ApJ, 520, L25
- Kocevski, D., Ryde, F., Liang, E. 2003, ApJ, 473, 998
- Krolik, J. H., and Pier, E. A. 1991, ApJ, 373, 277
- Liang, E. P., Jernigan, T. E., Rodrigues, R. 1983, ApJ, 271, 766
- McBreen, S., Quilligan, F., McBreen, B., Hanlon, L., and Watson, D. 2001, A&A, 380, L31
- McBreen, S., Quilligan, F., McBreen, B., Hanlon, L., and Watson, D. 2003, AIP Conf. Proc. 662, 280

- Meszaros, P., Rees, M. J. 1998, ApJ, 502, L105
- Nemiroff, R. J. 2000, ApJ, 544, 805
- Norris, J. P., Nemiroff, R. J., Bonnell, J. T. et al. 1996, ApJ, 459, 393
- Norris et al. 2000, ApJ, 534, 248
- Paczynski, B. 1986, ApJ, 308, L43
- Preece, R. D., Briggs, M. S., Mallozzi, R. S. et al. 2000, ApJS, 126, 19
- Qin, Y.-P. 2002, A&A, 396, 705
- Qin, Y.-P. 2003, A&A, 407, 393
- Qin, Y.-P., Zhang, Z.-B., Zhang, F.-W., Cui, X.-H. 2004, ApJ, in press (Paper I)
- Qin, Y.-P. 2004, astro-ph/0411365
- Ryde, F., Petrosian, V. 2002, ApJ, 473, 998
- Schaefer, B. E., Teegaeden, B. J., Fantasia, S. F. et al. 1994, ApJS, 92, 285

Table 1. Relative peak count rates and total counts of the light curves of Fig. 1

$\Delta\tau_{\theta,F}$	$ch$	$(Gau, \Gamma = 200)$		$(pow, \Gamma = 200)$		$(Gau, \Gamma = 20)$		$(pow, \Gamma = 20)$	
		$\frac{C_p}{C_{p,H}}$	$\frac{C_{total}}{C_{total,H}}$	$\frac{C_p}{C_{p,H}}$	$\frac{C_{total}}{C_{total,H}}$	$\frac{C_p}{C_{p,H}}$	$\frac{C_{total}}{C_{total,H}}$	$\frac{C_p}{C_{p,H}}$	$\frac{C_{total}}{C_{total,H}}$
0.01	$A$	1.27	1.68	1.27	1.75	7.51	14.7	7.54	15.4
	$B$	1.27	1.67	1.27	1.74	7.40	14.2	7.43	14.7
	$C$	1.27	1.66	1.27	1.73	7.22	13.4	7.25	13.8
	$D$	1.26	1.64	1.26	1.71	6.88	12.0	6.90	12.2
	$E$	1.24	1.59	1.24	1.64	5.95	8.95	5.97	9.00
	$F$	1.21	1.50	1.21	1.54	4.68	5.92	4.69	5.93
	$G$	1.16	1.34	1.16	1.36	2.92	3.07	2.92	3.07
	$H$	1.00	1.00	1.00	1.00	1.00	1.00	1.00	1.00
	$I$	0.787	0.662	0.786	0.659	0.420	0.420	0.420	0.420
	$J$	0.491	0.344	0.490	0.342	0.177	0.177	0.177	0.177
	$K$	0.168	0.112	0.168	0.111	0.0562	0.0562	0.0562	0.0562
0.1	$A$	1.29	1.66	1.30	1.76	7.89	14.6	8.19	15.4
	$B$	1.28	1.66	1.29	1.75	7.78	14.1	8.06	14.8
	$C$	1.28	1.65	1.29	1.74	7.58	13.3	7.85	13.9
	$D$	1.27	1.63	1.28	1.72	7.21	12.0	7.45	12.3
	$E$	1.25	1.58	1.26	1.65	6.20	8.94	6.37	9.00
	$F$	1.22	1.49	1.23	1.54	4.83	5.92	4.93	5.93
	$G$	1.16	1.34	1.17	1.36	2.95	3.07	2.97	3.07
	$H$	1.00	1.00	1.00	1.00	1.00	1.00	1.00	1.00
	$I$	0.779	0.662	0.773	0.658	0.420	0.420	0.420	0.420
	$J$	0.477	0.344	0.467	0.341	0.177	0.177	0.177	0.177
	$K$	0.162	0.112	0.157	0.111	0.0562	0.0562	0.0562	0.0562
1	$A$	1.30	1.76	1.35	1.78	8.33	15.4	9.45	15.6
	$B$	1.30	1.75	1.35	1.77	8.20	14.8	9.28	14.9
	$C$	1.30	1.74	1.34	1.76	7.98	13.8	9.00	13.9
	$D$	1.29	1.71	1.33	1.73	7.57	12.3	8.47	12.3
	$E$	1.27	1.64	1.31	1.66	6.46	9.00	7.09	9.01
	$F$	1.24	1.54	1.27	1.55	4.97	5.93	5.29	5.93
	$G$	1.17	1.36	1.20	1.36	2.98	3.07	3.03	3.07
	$H$	1.00	1.00	1.00	1.00	1.00	1.00	1.00	1.00
	$I$	0.770	0.658	0.747	0.658	0.420	0.420	0.420	0.420
	$J$	0.462	0.342	0.428	0.341	0.177	0.177	0.177	0.177
	$K$	0.155	0.111	0.141	0.111	0.0562	0.0562	0.0562	0.0562

Note:  $\Delta\tau_{\theta,F}$  —  $\Delta\tau_{\theta,FWHM}$ ,  $ch$  — channel,  $Gau$  — Gaussian pulse,  $pow$  — power law pulse.

Table 2. Relative peak count rates and total counts of the light curves of channels with larger energy ranges in the case of local Gaussian pulses

$\Delta\tau_{\theta,F}$	$ch$	( $\Gamma = 200$ )		( $\Gamma = 20$ )	
		$\frac{C_p}{C_{p,H}}$	$\frac{C_{total}}{C_{total,H}}$	$\frac{C_p}{C_{p,H}}$	$\frac{C_{total}}{C_{total,H}}$
0.01	<i>Aa</i>	1.68	2.22	9.91	19.4
	<i>Da</i>	1.67	2.17	8.98	15.5
	<i>Ga</i>	1.51	1.73	3.48	3.63
	<i>Ia</i>	1.11	0.895	0.542	0.542
	<i>Kb</i>	0.426	0.284	0.143	0.143
0.1	<i>Aa</i>	1.70	2.20	10.4	19.2
	<i>Da</i>	1.68	2.15	9.40	15.4
	<i>Ga</i>	1.52	1.72	3.51	3.63
	<i>Ia</i>	1.10	0.896	0.542	0.542
	<i>Kb</i>	0.410	0.284	0.143	0.143
1	<i>Aa</i>	1.72	2.32	11.0	20.3
	<i>Da</i>	1.70	2.26	9.86	15.7
	<i>Ga</i>	1.53	1.75	3.54	3.63
	<i>Ia</i>	1.08	0.891	0.542	0.542
	<i>Kb</i>	0.394	0.282	0.143	0.143

Table 3. Relative peak count rates and total counts of the light curves of various channels in the case of the local Gaussian pulse with  $\Delta\tau_{\theta,FWHM} = 0.1$  for the rest frame Band function spectrum with  $\alpha_0 = 0$  and  $\beta_0 = -3.5$

$ch$	$(\Gamma = 200)$		$(\Gamma = 20)$	
	$\frac{C_p}{C_{p,H}}$	$\frac{C_{total}}{C_{total,H}}$	$\frac{C_p}{C_{p,H}}$	$\frac{C_{total}}{C_{total,H}}$
$A$	0.00675	0.0188	0.398	2.91
$B$	0.0168	0.0463	0.964	6.31
$C$	0.0335	0.0902	1.83	10.2
$D$	0.0662	0.172	3.29	14.4
$E$	0.160	0.372	6.01	17.0
$F$	0.304	0.601	7.19	13.9
$G$	0.547	0.848	5.33	6.94
$H$	1.00	1.00	1.00	1.00
$I$	1.20	0.815	0.177	0.177
$J$	0.887	0.408	0.0313	0.0313
$K$	0.167	0.0588	0.00316	0.00316
$Aa$	0.0101	0.0282	0.595	4.30
$Da$	0.0990	0.253	4.77	19.8
$Ga$	0.793	1.16	6.20	7.86
$Ia$	1.79	1.11	0.201	0.202
$Kb$	0.608	0.231	0.0131	0.0132



Table 4. Relative peak count rates and total counts of the light curves of various channels in the case of the local Gaussian pulse with  $\Delta\tau_{\theta,FWHM} = 0.1$  for the rest frame Band function spectrum with  $\alpha_0 = -1.5$  and  $\beta_0 = -2$

$ch$	$(\Gamma = 200)$		$(\Gamma = 20)$	
	$\frac{C_p}{C_{p,H}}$	$\frac{C_{total}}{C_{total,H}}$	$\frac{C_p}{C_{p,H}}$	$\frac{C_{total}}{C_{total,H}}$
$A$	17.9	20.1	40.2	51.4
$B$	11.3	12.7	25.3	32.0
$C$	7.98	8.96	17.6	22.0
$D$	5.63	6.30	12.2	14.8
$E$	3.53	3.92	7.15	8.16
$F$	2.47	2.70	4.47	4.75
$G$	1.70	1.81	2.48	2.50
$H$	1.00	1.00	1.00	1.00
$I$	0.625	0.582	0.500	0.500
$J$	0.348	0.306	0.250	0.250
$K$	0.140	0.123	0.100	0.100
$Aa$	22.4	25.3	50.5	64.6
$Da$	7.06	7.91	15.2	18.4
$Ga$	2.12	2.26	2.98	3.00
$Ia$	0.857	0.789	0.667	0.669
$Kb$	0.327	0.287	0.233	0.235

Table 5. Relative peak count rates and total counts of the light curves of various channels in the case of the local Gaussian pulse with  $\Delta\tau_{\theta,FWHM} = 0.1$  for the rest frame thermal synchrotron spectrum

$ch$	$(\Gamma = 200)$		$(\Gamma = 20)$	
	$\frac{C_p}{C_{p,H}}$	$\frac{C_{total}}{C_{total,H}}$	$\frac{C_p}{C_{p,H}}$	$\frac{C_{total}}{C_{total,H}}$
$A$	0.0968	0.267	3.53	12.7
$B$	0.195	0.485	5.54	16.8
$C$	0.315	0.711	7.02	18.3
$D$	0.481	0.972	7.90	17.6
$E$	0.757	1.28	7.33	13.1
$F$	0.958	1.40	5.53	8.28
$G$	1.08	1.35	3.26	4.10
$H$	1.00	1.00	1.00	1.00
$I$	0.755	0.635	0.257	0.217
$J$	0.445	0.314	0.0397	0.0283
$K$	0.137	0.0766	0.00125	0.000719
$Aa$	0.141	0.384	4.98	17.5
$Da$	0.679	1.34	10.5	22.7
$Ga$	1.43	1.74	3.88	4.80
$Ia$	1.05	0.854	0.289	0.242
$Kb$	0.370	0.229	0.0105	0.00687

Table 6. Relative peak count rates and total counts of the light curves of various channels in the case of the local Gaussian pulse with  $\Delta\tau_{\theta,FWHM} = 0.1$  for the rest frame

Comptonized spectrum				
$ch$	$(\Gamma = 200)$		$(\Gamma = 20)$	
	$\frac{C_p}{C_{p,H}}$	$\frac{C_{total}}{C_{total,H}}$	$\frac{C_p}{C_{p,H}}$	$\frac{C_{total}}{C_{total,H}}$
$A$	0.156	0.263	2.88	13.4
$B$	0.224	0.377	4.07	18.0
$C$	0.295	0.492	5.19	21.3
$D$	0.386	0.634	6.38	23.3
$E$	0.545	0.853	7.47	21.1
$F$	0.695	1.01	6.98	15.2
$G$	0.854	1.10	4.70	7.48
$H$	1.00	1.00	1.00	1.00
$I$	0.935	0.720	0.0708	0.0494
$J$	0.629	0.354	0.000442	0.000218
$K$	0.134	0.0473	$2.15 \times 10^{-10}$	$7.35 \times 10^{-11}$
$Aa$	0.216	0.365	3.99	18.4
$Da$	0.534	0.872	8.66	30.8
$Ga$	1.16	1.46	5.53	8.53
$Ia$	1.35	0.972	0.0713	0.0503
$Kb$	0.457	0.202	$3.26 \times 10^{-6}$	$1.39 \times 10^{-6}$

Table 7. Relative peak count rates and total counts of the light curves of various channels in the case of the local Gaussian pulse with  $\Delta\tau_{\theta,FWHM} = 0.1$  for the rest frame varying

Band function spectrum				
$ch$	$(\Gamma = 200)$		$(\Gamma = 20)$	
	$\frac{C_p}{C_{p,H}}$	$\frac{C_{total}}{C_{total,H}}$	$\frac{C_p}{C_{p,H}}$	$\frac{C_{total}}{C_{total,H}}$
$A$	0.204	0.351	2.59	7.45
$B$	0.281	0.480	3.50	9.52
$C$	0.357	0.603	4.31	10.8
$D$	0.451	0.748	5.13	11.4
$E$	0.609	0.954	5.74	9.99
$F$	0.750	1.08	5.20	7.14
$G$	0.893	1.14	3.40	3.68
$H$	1.00	1.00	1.00	1.00
$I$	0.906	0.714	0.359	0.358
$J$	0.592	0.368	0.129	0.129
$K$	0.174	0.100	0.0333	0.0331
$Aa$	0.281	0.484	3.56	10.2
$Da$	0.621	1.02	6.92	14.9
$Ga$	1.20	1.50	4.01	4.30
$Ia$	1.30	0.971	0.450	0.451
$Kb$	0.477	0.278	0.0920	0.0921

Table 8. Values of  $\Delta C_{\text{max}}$  and  $\Delta S$  in the case of local Gaussian pulses for the rest frame  
Band function spectrum with  $\alpha_0 = -1$  and  $\beta_0 = -2.25$

$\Delta\tau_{\theta,F}$	$ch$	( $\Gamma = 200$ )		( $\Gamma = 20$ )	
		$\Delta C_{\max}$	$\Delta S$	$\Delta C_{\max}$	$\Delta S$
0.01	$A$	−0.07	−0.05	−1.34	−0.91
	$B$	−0.07	−0.05	−1.29	−0.88
	$C$	−0.07	−0.05	−1.23	−0.84
	$D$	−0.07	−0.04	−1.10	−0.75
	$E$	−0.06	−0.04	−0.78	−0.53
	$F$	−0.05	−0.03	−0.42	−0.28
	$G$	−0.04	−0.02	−0.08	−0.05
	$H$	0.00	0.00	0.00	0.00
	$I$	0.04	0.02	0.00	0.00
	$J$	0.05	0.04	0.00	0.00
	$K$	0.02	0.02	0.00	0.00
	$Aa$	−0.09	−0.06	−1.76	−1.21
	$Da$	−0.09	−0.06	−1.41	−0.96
	$Ga$	−0.04	−0.03	−0.08	−0.05
	$Ia$	0.07	0.05	0.00	0.00
	$Kb$	0.06	0.04	0.00	0.00
0.1	$A$	−0.08	−0.05	−1.51	−1.09
	$B$	−0.08	−0.05	−1.47	−1.05
	$C$	−0.07	−0.05	−1.39	−1.00
	$D$	−0.07	−0.05	−1.24	−0.89
	$E$	−0.07	−0.05	−0.88	−0.63
	$F$	−0.06	−0.04	−0.46	−0.33
	$G$	−0.04	−0.03	−0.08	−0.05
	$H$	0.00	0.00	0.00	0.00
	$I$	0.04	0.03	0.00	0.00
	$J$	0.06	0.04	0.00	0.00
	$K$	0.02	0.02	0.00	0.00
	$Aa$	−0.10	−0.07	−2.00	−1.44
	$Da$	−0.10	−0.07	−1.59	−1.14
	$Ga$	−0.05	−0.03	−0.08	−0.05
	$Ia$	0.08	0.05	0.00	0.00
	$Kb$	0.06	0.04	0.00	0.00
1	$A$	−0.08	−0.06	−1.71	−1.28
	$B$	−0.08	−0.06	−1.66	−1.24
	$C$	−0.08	−0.06	−1.57	−1.17
	$D$	−0.08	−0.06	−1.40	−1.04
	$E$	−0.07	−0.05	−0.98	−0.72
	$F$	−0.06	−0.05	−0.51	−0.37
	$G$	−0.04	−0.03	−0.08	−0.06
	$H$	0.00	0.00	0.00	0.00
	$I$	0.04	0.03	0.00	0.00

Table 9. Values of  $\Delta C_{\max}$  and  $\Delta S$  in the case of the local Gaussian pulse with  $\Delta\tau_{\theta,FWHM} = 0.1$  for the rest frame Band function spectrum with  $\alpha_0 = 0$  and  $\beta_0 = -3.5$

$ch$	$(\Gamma = 200)$		$(\Gamma = 20)$	
	$\Delta C_{\max}$	$\Delta S$	$\Delta C_{\max}$	$\Delta S$
$A$	0.00	0.00	−0.21	−0.15
$B$	0.00	0.00	−0.50	−0.35
$C$	−0.01	0.00	−0.92	−0.64
$D$	−0.01	−0.01	−1.55	−1.10
$E$	−0.03	−0.02	−2.36	−1.70
$F$	−0.05	−0.03	−2.11	−1.53
$G$	−0.06	−0.04	−0.81	−0.58
$H$	0.00	0.00	0.00	0.00
$I$	0.16	0.11	0.00	0.00
$J$	0.26	0.17	0.00	0.00
$K$	0.07	0.05	0.00	0.00
$Aa$	0.00	0.00	−0.31	−0.22
$Da$	−0.02	−0.01	−2.20	−1.56
$Ga$	−0.08	−0.05	−0.83	−0.59
$Ia$	0.31	0.21	0.00	0.00
$Kb$	0.23	0.16	0.00	0.00

Table 10. Values of  $\Delta C_{\max}$  and  $\Delta S$  in the case of the local Gaussian pulse with  $\Delta\tau_{\theta,FWHM} = 0.1$  for the rest frame Band function spectrum with  $\alpha_0 = -1.5$  and  $\beta_0 = -2$

$ch$	$(\Gamma = 200)$		$(\Gamma = 20)$	
	$\Delta C_{\max}$	$\Delta S$	$\Delta C_{\max}$	$\Delta S$
$A$	−0.42	−0.30	−2.96	−2.13
$B$	−0.27	−0.19	−1.83	−1.31
$C$	−0.19	−0.13	−1.23	−0.88
$D$	−0.13	−0.09	−0.79	−0.57
$E$	−0.08	−0.05	−0.37	−0.26
$F$	−0.05	−0.03	−0.14	−0.10
$G$	−0.02	−0.02	−0.01	−0.01
$H$	0.00	0.00	0.00	0.00
$I$	0.01	0.01	0.00	0.00
$J$	0.02	0.01	0.00	0.00
$K$	0.01	0.01	0.00	0.00
$Aa$	−0.53	−0.37	−3.71	−2.66
$Da$	−0.16	−0.11	−0.98	−0.70
$Ga$	−0.03	−0.02	−0.01	−0.01
$Ia$	0.03	0.02	0.00	0.00
$Kb$	0.02	0.01	0.00	0.00



Table 11. Values of  $\Delta C_{\max}$  and  $\Delta S$  in the case of the local Gaussian pulse with  $\Delta\tau_{\theta,FWHM} = 0.1$  for the rest frame thermal synchrotron spectrum

$ch$	$(\Gamma = 200)$		$(\Gamma = 20)$	
	$\Delta C_{\max}$	$\Delta S$	$\Delta C_{\max}$	$\Delta S$
$A$	−0.02	−0.02	−1.29	−0.92
$B$	−0.05	−0.03	−1.82	−1.30
$C$	−0.07	−0.05	−2.07	−1.49
$D$	−0.09	−0.06	−2.03	−1.46
$E$	−0.11	−0.08	−1.44	−1.05
$F$	−0.10	−0.07	−0.80	−0.58
$G$	−0.07	−0.05	−0.28	−0.20
$H$	0.00	0.00	0.00	0.00
$I$	0.04	0.03	0.02	0.01
$J$	0.05	0.04	0.01	0.00
$K$	0.03	0.02	0.00	0.00
$Aa$	−0.04	−0.02	−1.79	−1.27
$Da$	−0.12	−0.09	−2.61	−1.89
$Ga$	−0.08	−0.06	−0.31	−0.22
$Ia$	0.07	0.05	0.02	0.02
$Kb$	0.06	0.04	0.00	0.00

Table 12. Values of  $\Delta C_{\max}$  and  $\Delta S$  in the case of the local Gaussian pulse with  $\Delta\tau_{\theta,FWHM} = 0.1$  for the rest frame Comptonized spectrum

$ch$	$(\Gamma = 200)$		$(\Gamma = 20)$	
	$\Delta C_{\max}$	$\Delta S$	$\Delta C_{\max}$	$\Delta S$
$A$	−0.02	−0.01	−1.25	−0.89
$B$	−0.02	−0.02	−1.75	−1.24
$C$	−0.03	−0.02	−2.18	−1.55
$D$	−0.04	−0.03	−2.59	−1.84
$E$	−0.05	−0.03	−2.71	−1.95
$F$	−0.05	−0.04	−2.09	−1.52
$G$	−0.05	−0.03	−0.94	−0.69
$H$	0.00	0.00	0.00	0.00
$I$	0.07	0.05	0.01	0.01
$J$	0.12	0.08	0.00	0.00
$K$	0.05	0.04	0.00	0.00
$Aa$	−0.02	−0.01	−1.73	−1.22
$Da$	−0.05	−0.04	−3.48	−2.48
$Ga$	−0.06	−0.04	−1.02	−0.75
$Ia$	0.14	0.10	0.01	0.01
$Kb$	0.13	0.09	0.00	0.00

Table 13. Values of  $\Delta C_{\max}$  and  $\Delta S$  in the case of the local Gaussian pulse with  $\Delta\tau_{\theta,FWHM} = 0.1$  for the rest frame varying Band function spectrum

$ch$	$(\Gamma = 200)$		$(\Gamma = 20)$	
	$\Delta C_{\max}$	$\Delta S$	$\Delta C_{\max}$	$\Delta S$
$A$	−0.03	−0.02	−0.82	−0.62
$B$	−0.03	−0.03	−1.08	−0.81
$C$	−0.04	−0.03	−1.28	−0.95
$D$	−0.05	−0.04	−1.42	−1.05
$E$	−0.06	−0.04	−1.31	−0.96
$F$	−0.06	−0.05	−0.84	−0.61
$G$	−0.05	−0.04	−0.21	−0.14
$H$	0.00	0.00	0.00	0.00
$I$	0.07	0.05	0.00	0.00
$J$	0.11	0.08	0.00	0.00
$K$	0.04	0.03	0.00	0.00
$Aa$	−0.03	−0.03	−1.13	−0.85
$Da$	−0.07	−0.05	−1.89	−1.40
$Ga$	−0.06	−0.05	−0.21	−0.14
$Ia$	0.14	0.10	0.01	0.00
$Kb$	0.11	0.08	0.00	0.00

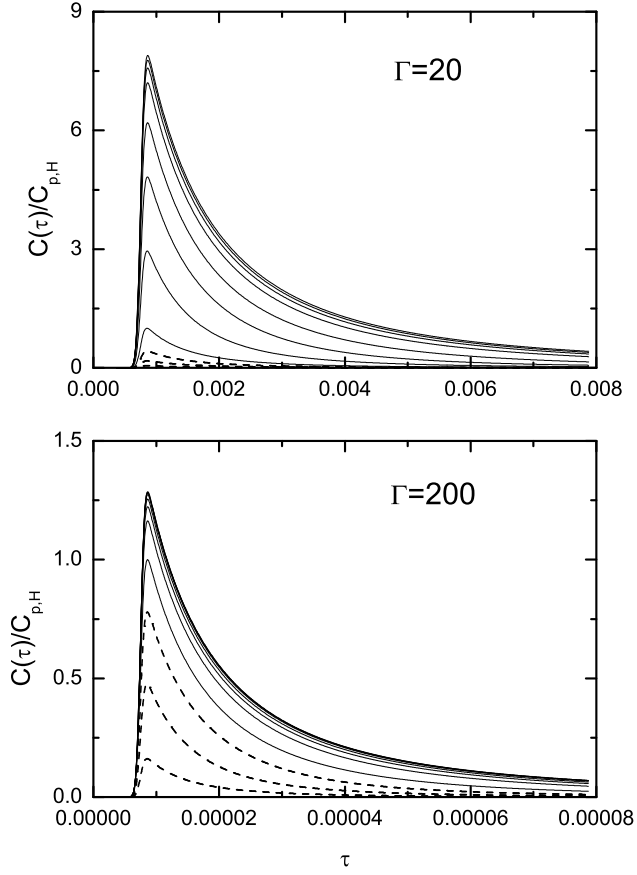


Fig. 1. — Light curves (solid lines) of channels A, B, C, D, E, F, G, and H, and those (dash lines) of channels I, J, and K for the typical hard (the lower panel) and soft (the upper panel) bursts, calculated with (A1), arising from the local Gaussian pulse with  $\Delta\tau_{\theta,FWHM} = 0.1$  and the rest frame Band function with  $\nu_{0,p} = 0.75keVh^{-1}$ ,  $\alpha_0 = -1$  and  $\beta_0 = -2.25$ , where  $C_{p,H}$  is the peak count rate of channel H.

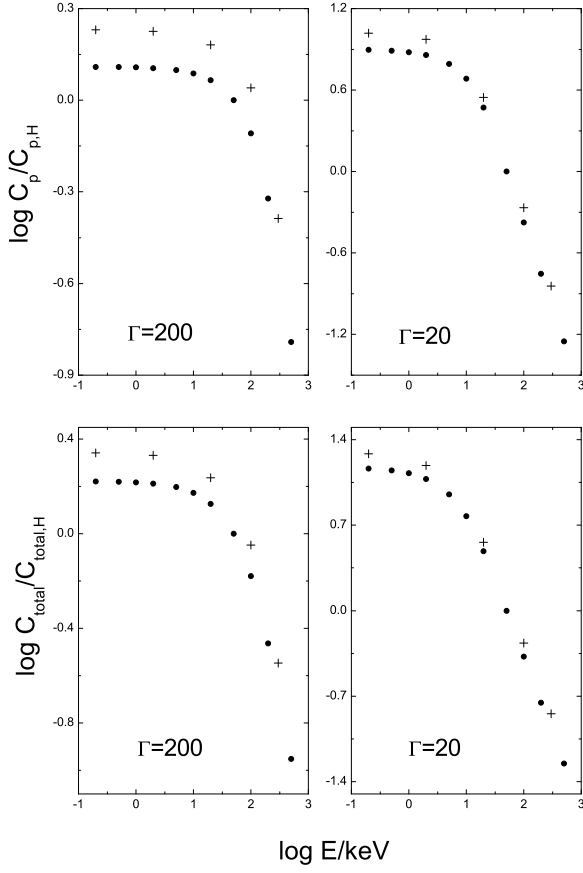


Fig. 2. — Relationships between the peak count rate and energy (upper panels) and between the total count and energy (lower panels), of the light curves arising from the local Gaussian pulse with  $\Delta\tau_{\theta,FWHM} = 0.1$  and the rest frame Band function with  $\nu_{0,p} = 0.75\text{keVh}^{-1}$ ,  $\alpha_0 = -1$  and  $\beta_0 = -2.25$ , for the typical hard (left panels) and soft (right panels) bursts, respectively, where  $C_{\text{total},H}$  is the total count of channel H. Filled circles represent channels A, B, C, D, E, F, G, H, I, J, and K, and pluses sand for channels Aa, Da, Ga, Ia, and Kb.

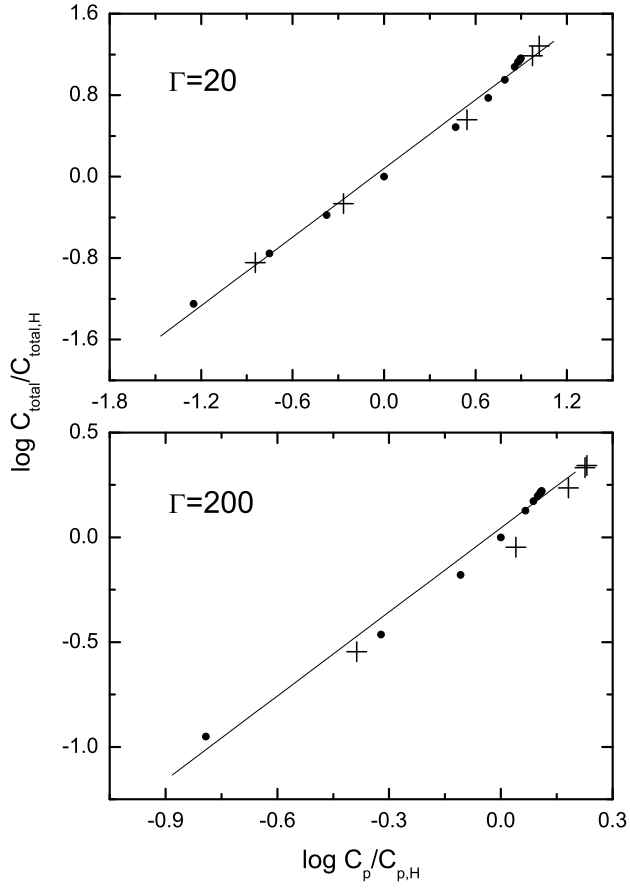


Fig. 3. — Relationship between the peak count rate and the total count of the light curves arising from the local Gaussian pulse with  $\Delta\tau_{\theta,FWHM} = 0.1$  and the rest frame Band function with  $\nu_{0,p} = 0.75 \text{ keV h}^{-1}$ ,  $\alpha_0 = -1$  and  $\beta_0 = -2.25$ , for the typical hard (the lower panel) and soft (the upper panel) bursts, respectively, where solid lines are the corresponding regression lines and other symbols are the same as those adopted in Fig. 2.

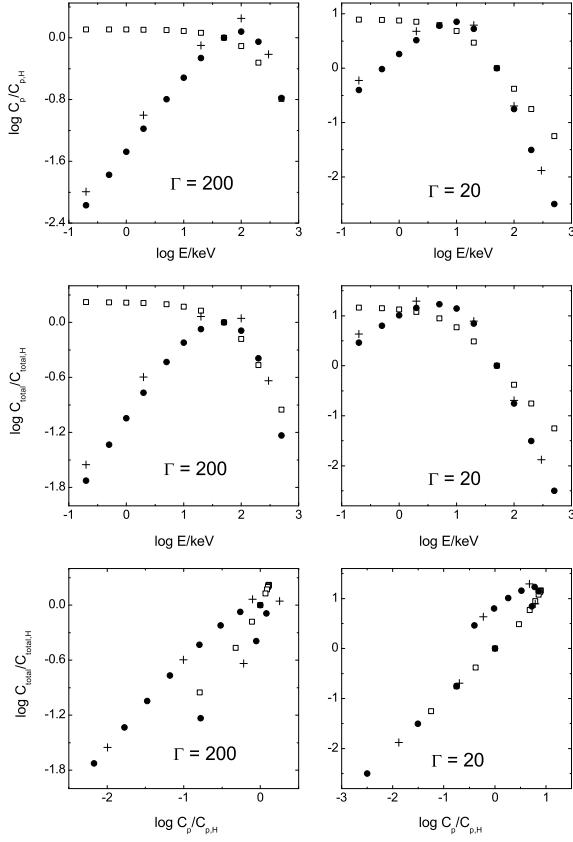


Fig. 4. — Relationships between the peak count rate and energy (the first row panels), and between the total count and energy (the second row panels), and between the peak count rate and the total count (the third row panels), of the light curves arising from the local Gaussian pulse with  $\Delta\tau_{\theta,FWHM} = 0.1$  and the rest frame Band function with  $\nu_{0,p} = 0.75 \text{keVh}^{-1}$ ,  $\alpha_0 = 0$  and  $\beta_0 = -3.5$ , for the typical hard (left panels) and soft (right panels) bursts, respectively. Open squares denote the filled circles in Figs. 2 and 3. Filled circles represent channels A, B, C, D, E, F, G, H, I, J, and K, and pluses sand for channels Aa, Da, Ga, Ia, and Kb.

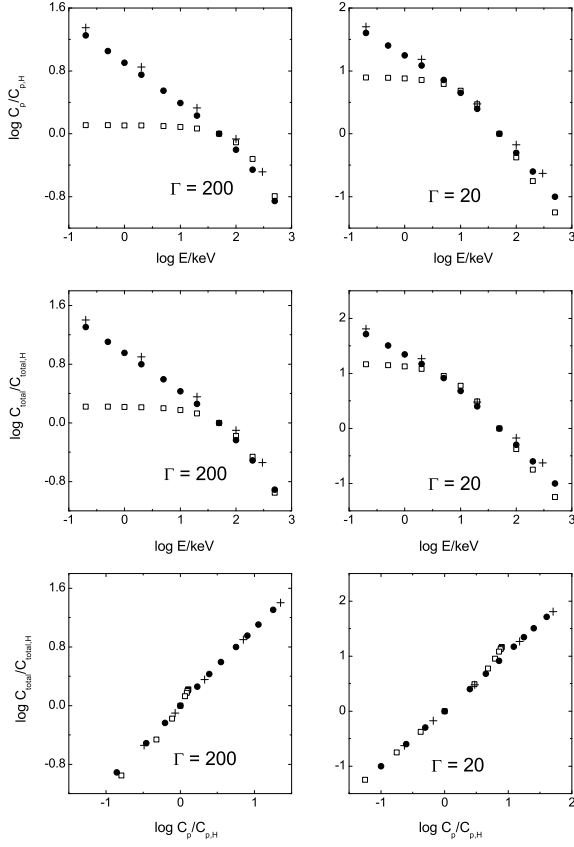


Fig. 5. — Relationships between the peak count rate and energy (the first row panels), and between the total count and energy (the second row panels), and between the peak count rate and the total count (the third row panels), of the light curves arising from the local Gaussian pulse with  $\Delta\tau_{\theta,FWHM} = 0.1$  and the rest frame Band function with  $\nu_{0,p} = 0.75 \text{keVh}^{-1}$ ,  $\alpha_0 = -1.5$  and  $\beta_0 = -2$ , for the typical hard (left panels) and soft (right panels) bursts, respectively. The symbols are the same as those adopted in Fig. 4.



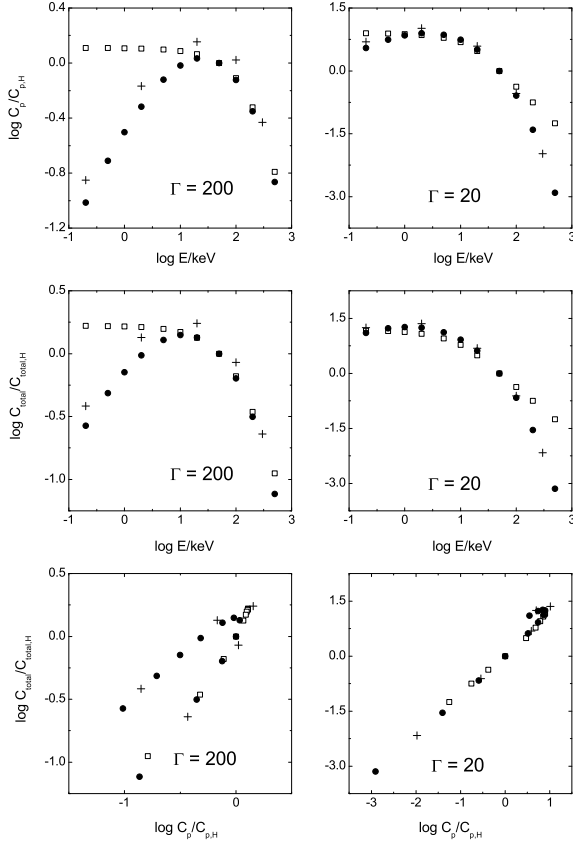


Fig. 6. — Relationships between the peak count rate and energy (the first row panels), and between the total count and energy (the second row panels), and between the peak count rate and the total count (the third row panels), of the light curves arising from the local Gaussian pulse with  $\Delta\tau_{\theta,FWHM} = 0.1$  and the rest frame thermal synchrotron spectrum with  $\nu_{0,s} = 3.5 \times 10^{-3} \text{keVh}^{-1}$ , for the typical hard (left panels) and soft (right panels) bursts, respectively. The symbols are the same as those adopted in Fig. 4.

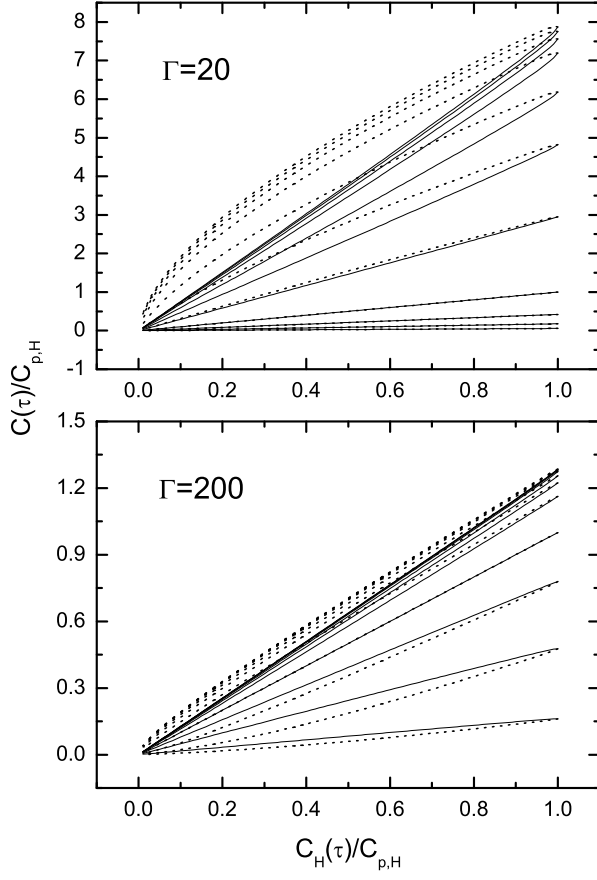


Fig. 7. — Plot of  $C(\tau)$  versus  $C_H(\tau)$  deduced from the light curves of Fig.1, where  $C(\tau)$  denotes the count rate of channels A, B, C, D, E, F, G, H, I, J, and K, and  $C_H(\tau)$  represents the count rate of channel H. The solid line and the dot line correspond to the rising portion and the decaying phase of the light curves, respectively.

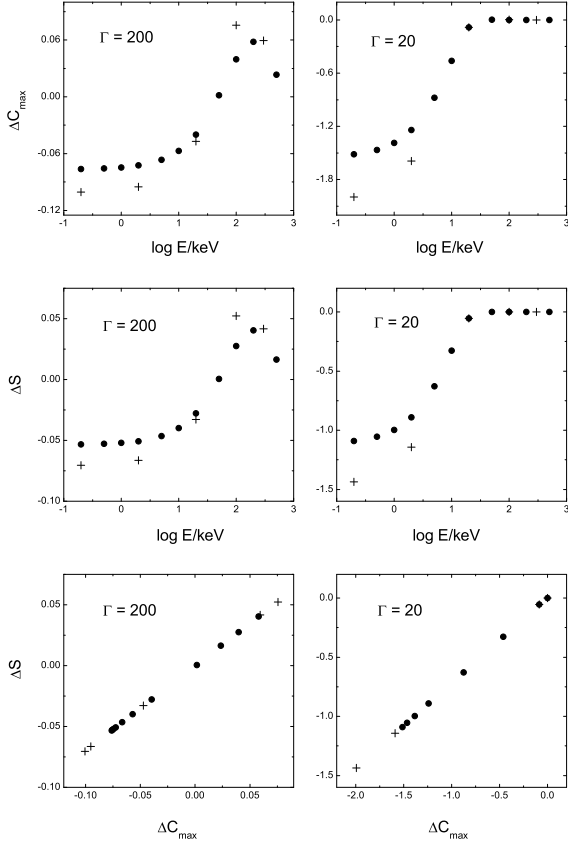


Fig. 8. — Relationships between  $\Delta C_{\max}$  and energy (the first row panels), and between  $\Delta S$  and energy (the second row panels), and between  $\Delta C_{\max}$  and  $\Delta S$  (the third row panels), of the light curves arising from the local Gaussian pulse with  $\Delta\tau_{\theta,FWHM} = 0.1$  and the rest frame Band function with  $\nu_{0,p} = 0.75\text{keV}h^{-1}$ ,  $\alpha_0 = -1$  and  $\beta_0 = -2.25$ , for the typical hard (left panels) and soft (right panels) bursts, respectively. Filled circles represent channels A, B, C, D, E, F, G, H, I, J, and K, and pluses sand for channels Aa, Da, Ga, Ia, and Kb.

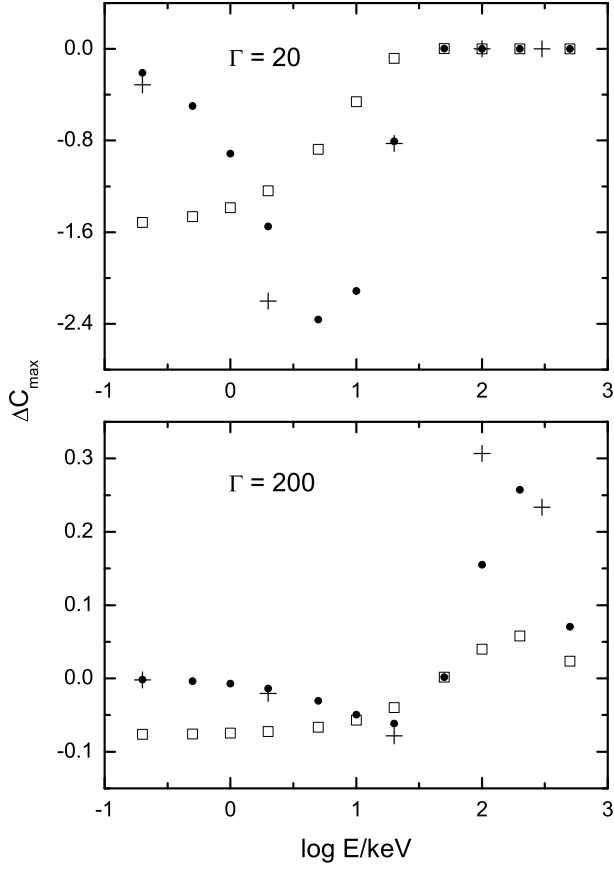


Fig. 9. — Relationship between  $\Delta C_{\max}$  and energy obtained from the light curves arising from the local Gaussian pulse with  $\Delta\tau_{\theta,FWHM} = 0.1$  and the rest frame Band function with  $\nu_{0,p} = 0.75 \text{ keV h}^{-1}$ ,  $\alpha_0 = 0$  and  $\beta_0 = -3.5$ , for the typical hard (the lower panel) and soft (the upper panel) bursts, respectively. Open squares denote the filled circles in the first row panels of Fig. 8. Filled circles represent channels A, B, C, D, E, F, G, H, I, J, and K, and pluses stand for channels Aa, Da, Ga, Ia, and Kb.

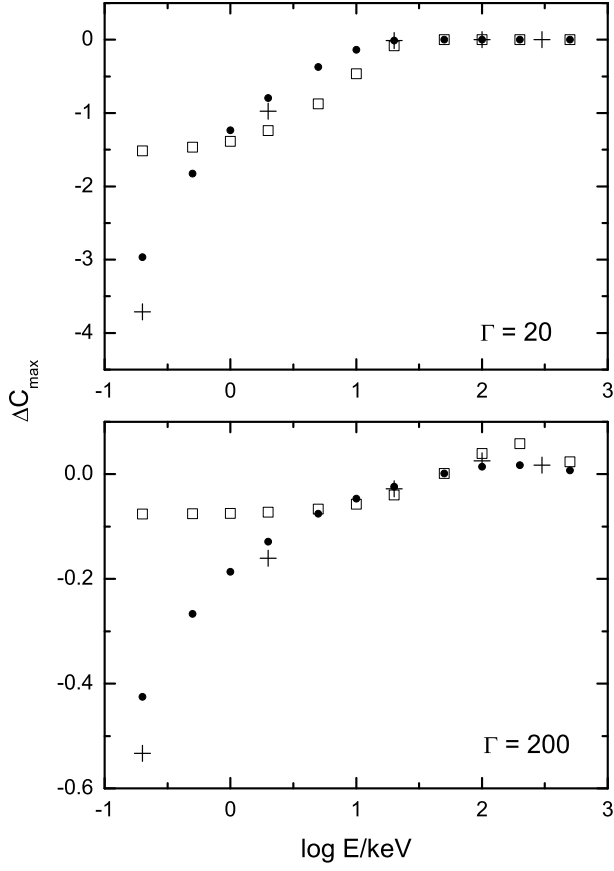


Fig. 10. — Relationship between  $\Delta C_{\max}$  and energy obtained from the light curves arising from the local Gaussian pulse with  $\Delta\tau_{\theta,FWHM} = 0.1$  and the rest frame Band function with  $\nu_{0,p} = 0.75\text{keVh}^{-1}$ ,  $\alpha_0 = -1.5$  and  $\beta_0 = -2$ , for the typical hard (the lower panel) and soft (the upper panel) bursts, respectively. The symbols are the same as those adopted in Fig. 9.

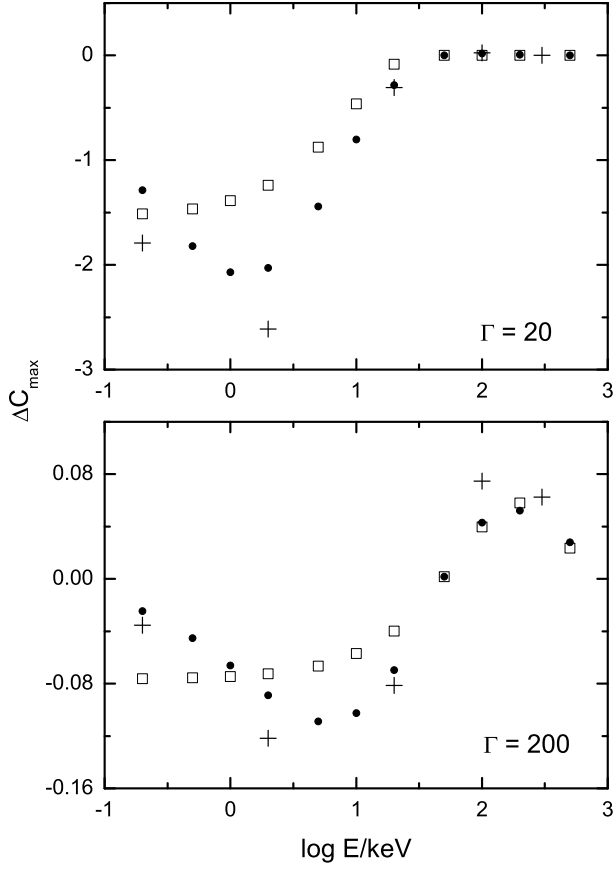


Fig. 11. — Relationship between  $\Delta C_{\max}$  and energy obtained from the light curves arising from the local Gaussian pulse with  $\Delta\tau_{\theta,FWHM} = 0.1$  and the rest frame thermal synchrotron spectrum with  $\nu_{0,s} = 3.5 \times 10^{-3} keVh^{-1}$ , for the typical hard (the lower panel) and soft (the upper panel) bursts, respectively. The symbols are the same as those adopted in Fig. 9.

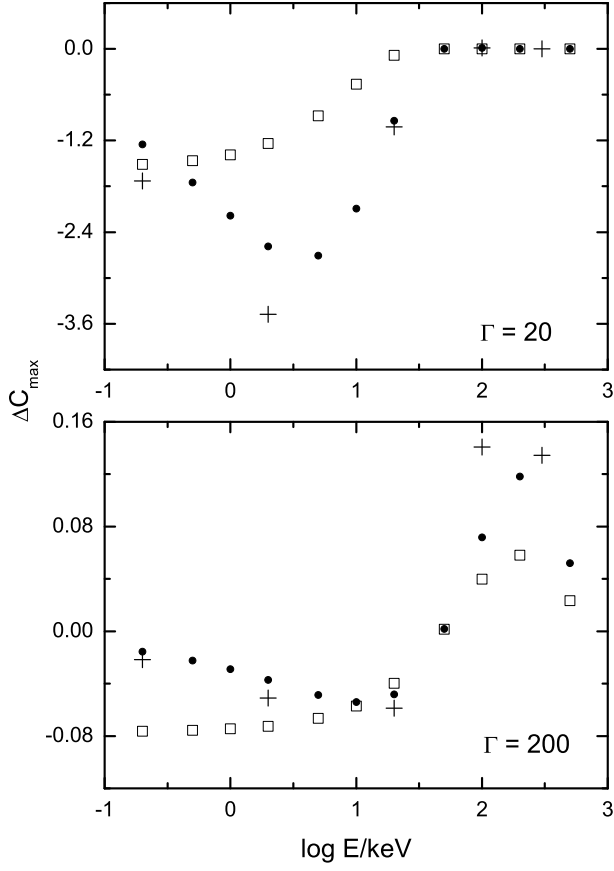


Fig. 12. — Relationship between  $\Delta C_{\max}$  and energy obtained from the light curves arising from the local Gaussian pulse with  $\Delta\tau_{\theta,FWHM} = 0.1$  and the rest frame Comptonized spectrum with  $\alpha_{0,C} = -0.6$  and  $\nu_{0,C} = 0.55\text{keV}h^{-1}$  for the typical hard (the lower panel) and soft (the upper panel) bursts, respectively. The symbols are the same as those adopted in Fig. 9.

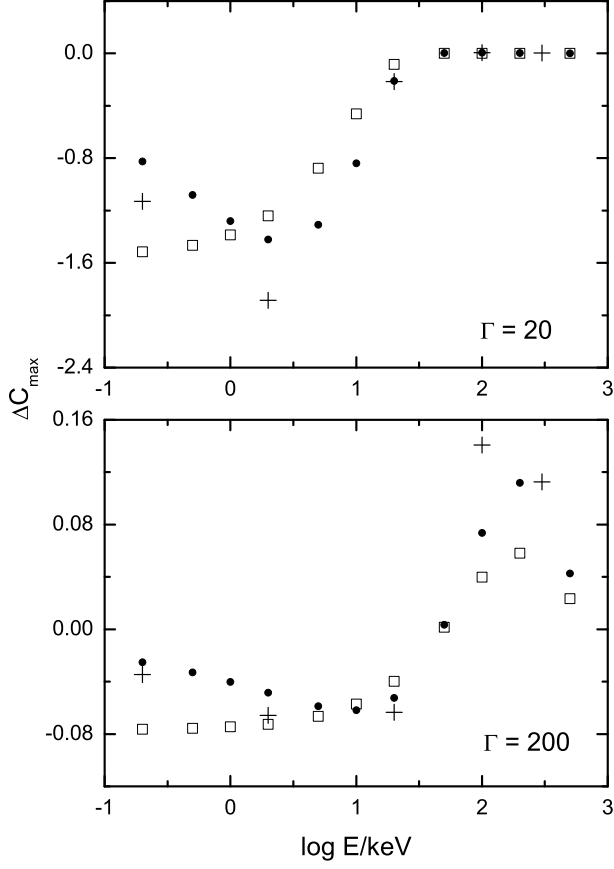


Fig. 13. — Relationship between  $\Delta C_{\max}$  and energy obtained from the light curves arising from the local Gaussian pulse with  $\Delta\tau_{\theta,FWHM} = 0.1$  and  $\tau_{\theta,0} = \tau_{\theta,\min}$ , and the rest frame varying Band function with  $\nu_{0,p} = 0.75 \text{ keV h}^{-1}$ ,  $\alpha_0 = -0.63 - 0.20(\tau_{\theta} - \tau_{\theta,\min})/6\sigma$ , and  $\beta_0 = -2.44 - 0.42(\tau_{\theta} - \tau_{\theta,\min})/6\sigma$ , for the typical hard (the lower panel) and soft (the upper panel) bursts, respectively. The symbols are the same as those adopted in Fig. 9.